

Compressional to shear wave conversion in oceanic crust

Robert S. White^{*} and Ralph A. Stephen

Woods Hole Oceanographic Institution, Woods Hole, Massachusetts 02543, USA

Received 1980 March 20; in original form 1979 November 22

Summary. Mode conversion for compressional to shear waves or vice versa, occurs most efficiently where the seismic wave encounters a large change in seismic velocities over a distance of less than half a wavelength. In the oceanic crust, the interface between water or sediment and the volcanic basement is frequently the site of considerable mode conversion. We examine the effect of changes in the sediment and the basement properties on the efficiency of mode conversion over a range of horizontal phase velocities assuming that the interface is a first order discontinuity. We then show with the aid of synthetic seismograms calculated using the reflectivity method that a small transition zone at the top of the basement over which the velocities increase with depth may have a considerable effect on the amount of conversion. In particular, small changes in the shear wave velocity structure over thicknesses of around half the shear wavelength may markedly change the amplitudes of the variable angle basement reflection and the doubly converted lower crustal shear waves even though we may only consider compressional waves incident on and returned from the crust. Thus, at typical seismic source frequencies, a change of only a few metres to a few tens of metres in the shear wave transition zone thickness, although considerably less than the wavelength of an incident compressional wave may greatly alter the resultant compressional wave crustal seismogram.

1 Introduction

In an earlier paper, White (1979), showed that the variation with range of the amplitude of the variable angle reflection off the top of the oceanic basement ('layer 2') is dependent not only on the velocity structure in the overlying sediments but also on the velocity variations in the upper part of the basement. In particular, one initially surprising result of theoretical seismogram modelling is that the fine-scale shear wave velocity structure of the basement has a marked effect on the variable angle *P*-wave reflections off the top of the basement.

^{*} Present address: Department of Geodesy and Geophysics, University of Cambridge, Madingley Rise, Madingley Road, Cambridge CB3 0EZ.

This is true even though both the incident and the reflected energy travels as *P*-waves, and even though the variations in shear wave velocity may occur over a depth of considerably less than one wavelength of the incident *P*-wave.

In this paper we first explore the effects of the seismic properties near the interface of the sediment or water and the underlying volcanic basement on the efficiency of mode conversion (*P* to *S* and *S* to *P*) at an interface between two half-spaces. We then use synthetic seismogram models of the response of a hydrophone in the water layer to investigate the way in which upper basement transition zones (over which the seismic velocities increase rapidly with depth), control the amplitudes of wide angle compressional reflections off the basement and of doubly converted lower crustal shear wave returns. Synthetic seismograms generated from a variety of other sediment and basement velocity models are discussed by Spudich & Helmberger (1979) and White (1979).

Doubly converted crustal shear waves have frequently been reported on marine seismic profiles recorded with a hydrophone in the water (e.g. Officer, Ewing & Wuenschel 1952; Ewing, Sutton & Officer 1954; Katz & Ewing 1956; Ewing & Ewing 1959; Cook, Algermissen & Costain 1962; Ludwig, Den & Murauchi 1973; Francis & Shor 1966; Murauchi *et al.* 1968; Helmberger & Morris 1970; Davis, Lister & Lewis 1976; Lewis & McClain 1977; Purdy & Detrick 1978; Spudich, Salisbury & Orcutt 1978; White 1979). Conversion from incident *P* to *S* and back from *S* to *P* occurs most efficiently at a sharp interface with a large contrast of seismic properties on either side. The most likely candidate in normal oceanic crust is the interface between water or sediment and the top of the volcanic basement. Little conversion would be expected at a sedimentary seafloor unless the sediments were unusually well consolidated or had high seismic velocities; in the succeeding discussion we will only consider conversion at the top of the volcanic basement, although the general conclusions are also applicable to any other major interface.

2 Factors affecting mode conversion

Conversion from compressional to shear energy and vice versa is a fickle phenomenon; strong doubly converted *S*-waves may be observed on one marine seismic profile but be absent from a nearby one. Some of the reasons may be:

(a) Rugged basement relief, such as that found in the North Atlantic, may prevent the downward propagating converted shear waves from being phase coherent, particularly where the variations in basement depth are on the same scale as the seismic wavelength (say 200 m for a typical marine seismic profile). Similarly, relief on an appropriate scale may destroy the phase coherency of *P*-waves converted at the basement from upward propagating shear waves. So although the properties at the basement interface may be appropriate for considerable mode conversion to occur, we may not see doubly converted *S*-waves as coherent arrivals.

(b) If the *P*-wave velocity in the sedimentary section exceeds the *S*-wave velocity in the underlying basement no doubly converted crustal shear waves will be returned (Spudich & Helmberger 1979).

(c) At an interface between two half-spaces the efficiency of mode conversion is dependent on the *P*- and *S*-wave velocities, the densities and the absorptivities of the two media, as discussed in Section 3. Lateral variations in the seismic properties of the volcanic basement and the overlying material will cause variability in the amplitudes of doubly converted crustal shear waves.

(d) In many instances the top of the volcanic basement cannot be considered as a first

order discontinuity at typical seismic wavelengths, but rather as a transition zone over which the velocities change (usually increase), with depth. This transition zone affects both the reflected and the transmitted energy in ways we explore in Sections 4 and 5, respectively.

3 *P*- to *S*-wave conversion at an interface

Before we discuss *P*- to *S*-wave conversion in velocity gradients, it is instructive to consider the simple case of wave conversion at an interface between two half-spaces. In this section we demonstrate the effect on the two-way conversion coefficient of varying the *P*- and *S*-wave velocities and the absorptivities in the two media using ranges of values typical of those found at the interface between water or sediment and layer 2. The *P* to *S* transmission coefficients were calculated from the displacement coefficients given by Červený & Ravindra (1971, equation 2.74); using their nomenclature R_{14} represents the coefficient describing conversion from incident *P*-wave in medium 1 to transmitted *S*-wave in medium 2 and R_{41} the reverse path. The proportion E_{ps} of the *P*-wave energy incident at angle θ_1 in medium 1 which is converted to *S*-wave energy at angle δ_2 in medium 2 is given by

$$E_{ps} = \frac{\rho_2 \beta_2^2}{\rho_1 \alpha_1^2} \cdot \frac{\cot \delta_2}{\cot \theta_1} \cdot R_{14}^2 \quad (1)$$

where α , β and ρ are the *P*- and *S*-wave velocities and the density, respectively in the half-space denoted by the subscript.

Since we are interested primarily in the signal received by a hydrophone in the water layer, we have plotted E_{psp} , the proportion of the incident *P*-wave energy at some angle of incidence which is converted to *S*-wave at the basement on its downward path, then converted back to *P*-wave on its return journey through the same interface. Then:

$$E_{psp} = R_{14}^2 \cdot R_{41}^2. \quad (2)$$

The two-way energy transmission coefficient E_{psp} represents the efficiency of *PSP* conversion at an interface between two half-spaces. It is important to note, however, that on a marine seismic profile the amplitudes of doubly converted shear waves depend not only on the efficiency of conversion at the basement interface but also on the crustal *S*-wave velocity structure which is responsible for turning the converted *S*-wave energy back toward the surface and which, together with crustal absorptivity, may cause further loss of energy. Thus the E_{psp} curves represent the upper bounds on the doubly converted energy; although we may conclude that if little or no energy is mode converted at the basement interface then we can be certain that no doubly converted shear wave arrivals will be observed on a marine profile, the converse is not necessarily true.

Spudich (1979), has shown that it is useful to view the transmission coefficient as a function of the horizontal phase velocity of the wave rather than of its angle of incidence because then the relationship is more apparent between the velocities on either side of the interface and the amount of energy potentially present in doubly converted crustal shear waves. Accordingly, our figures show the proportion of doubly converted energy E_{psp} at horizontal phase velocities up to 5 km s^{-1} . This range encompasses the phase velocities of all the major shear arrivals typically observed on marine profiles, including most notably the layer 3 refracted arrival of $3.6\text{--}3.9 \text{ km s}^{-1}$ and the mantle refraction of $4.5\text{--}4.8 \text{ km s}^{-1}$ (see, e.g. Christensen & Salisbury 1975, for a compilation; also Fowler 1976; Purdy & Detrick 1978; Spudich *et al.* 1978; Stephen, Loudon & Matthews 1980; White 1979).

In our discussion of the effects of varying the properties on either side of the interface, we will consider first the effect of varying the basement velocities with either water ($\alpha_1 = 1.50$, $\beta_1 = 0$ km s⁻¹) or unconsolidated sediment ($\alpha_1 = 2.0$, $\beta_1 = 0.5$ km s⁻¹) in the upper medium (Sections 3.1, 3.2). Secondly we will hold the basement velocities constant at representative values of $\alpha_2 = 4.5$, $\beta_2 = 2.6$ km s⁻¹ and show the effect of varying the velocities in the overlying medium (Sections 3.3, 3.4). Last, we discuss the effect of introducing absorption (Section 3.5).

3.1 BASEMENT WITH VARIABLE VELOCITIES BUT CONSTANT POISSON'S RATIO

The basement *P*-wave velocity, α_2 , has an important control on the efficiency of mode conversion at different phase velocities. When the overlying material is water, conversion to shear-wave energy is most efficient in a band of horizontal phase velocities below α_2 (Fig. 1). For example, with an α_2 of 4.0 km s⁻¹ over 35 per cent of the incident *P*-wave energy may be doubly converted at a typical layer 3 *S*-wave velocity of 3.8 km s⁻¹, whilst when α_2 is below 3.8 km s⁻¹, less than 7 per cent of the energy is available to travel via a converted *S*-wave mode. Furthermore, the two-way energy transmission coefficient drops rapidly to zero at a horizontal phase velocity equal to the basement *P*-wave velocity.

Replacing the water above the basement by unconsolidated sediment gives the same pattern of decreasing energy conversion at horizontal phase velocities greater than α_2 (Fig. 2a). As in all the figures we have only plotted curves for phase velocities which have real angles of incidence, δ_2 , in the lower medium (i.e. angles less than the *S*-wave critical angle).

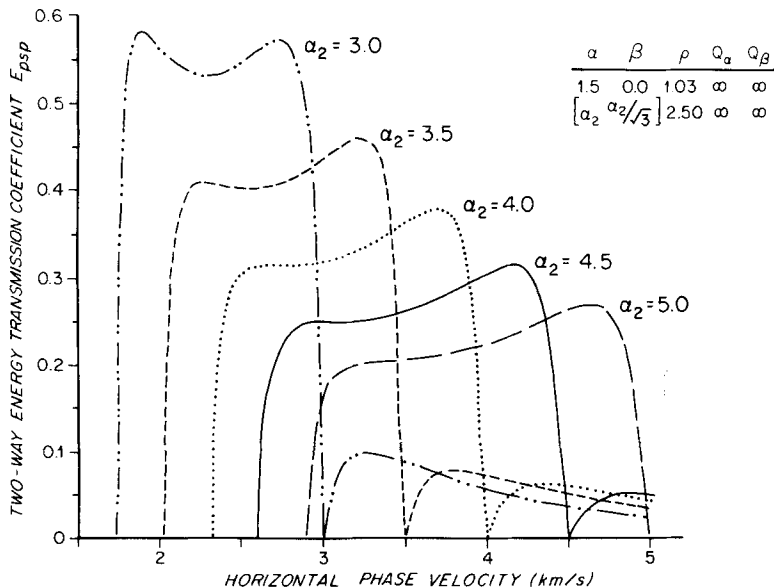


Figure 1. Basement with variable velocities but constant Poisson's ratio beneath water. Two-way energy transmission coefficient E_{psp} for doubly converted waves is plotted versus horizontal phase velocity. Calculated using Červený & Ravindra (1971) displacement coefficients for an interface between two half-spaces with *P*-waves incident in the upper medium. Note the decrease in efficiency of energy conversion at phase velocities greater than the basement *P*-wave velocity. In the annotation of Figs 1–7, inclusive, α and β are the *P*- and *S*-wave velocities in km s⁻¹, ρ the density in g cm⁻³, Q_α and Q_β the *P*- and *S*-wave quality factors. Subscripts 1 or 2 refer to the upper or lower half-spaces respectively.

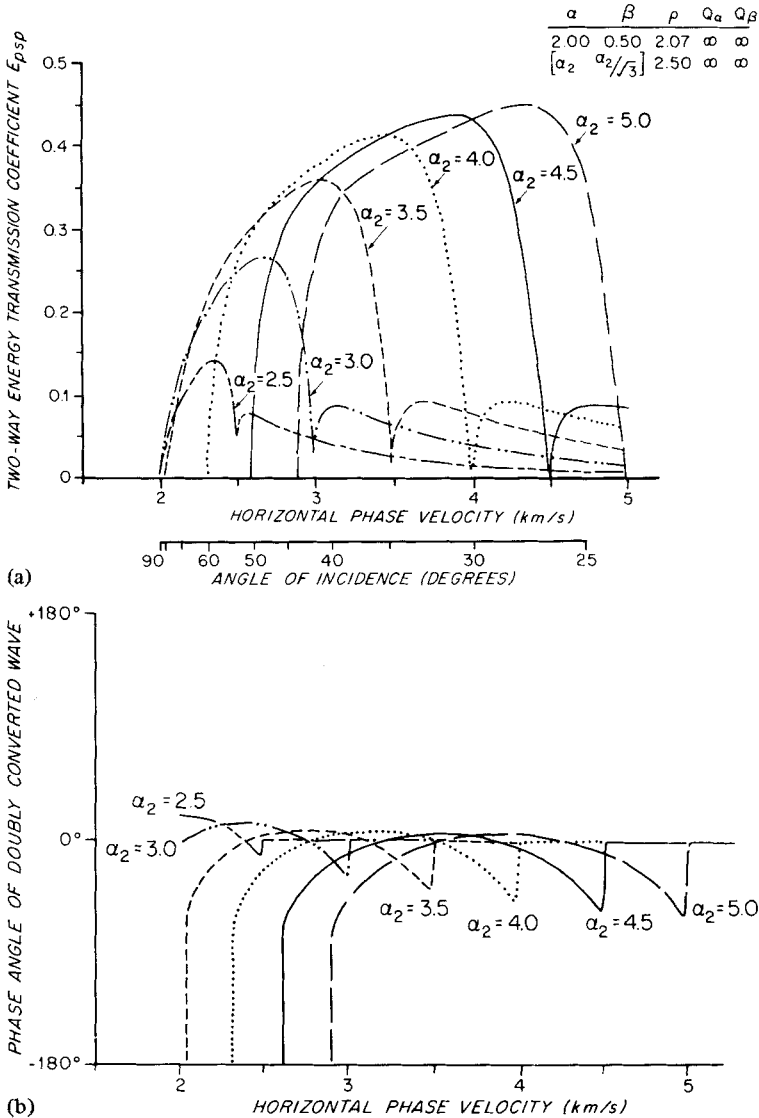


Figure 2. Basement with variable velocities but constant Poisson's ratio, beneath an unconsolidated sediment. (a) Two-way energy conversion coefficient E_{psp} at an interface between two half-spaces plotted versus the horizontal phase velocity; the angle of incidence on the interface in the upper medium is also shown. (b) Phase angle of the doubly converted wave with respect to the phase of the P-wave incident in the upper medium. Note the decreased efficiency of energy conversion at phase velocities greater than the basement P-wave velocity (as in Fig. 1), and the small change in phase angle of the doubly converted wave other than near the critical phase velocities.

Thus the lower limit of the curves, at which the converted energy drops to zero, is either the velocity α_1 (2.0 km s⁻¹ in Fig. 2), or the basement shear wave velocity β_2 when it is higher than α_1 . These curves then represent energy transmission coefficients for converted shear body waves propagating through the basement. The two-way conversion efficiency decreases monotonically as the horizontal phase velocity increases to very high values (i.e. angle of incidence decreases), until at normal incidence (infinite phase velocity), there is zero mode conversion.

We also note that in the example shown the phase angle of the doubly converted wave with respect to the phase angle of the incident P -wave varies little over the range of horizontal phase velocities relevant to crustal shear waves (Fig. 2b), even near the P -wave critical angle (where the incident phase velocity = α_2). Thus the phase angle of the doubly converted wave is not greatly changed by lateral variations in the basement velocity. This is important because with near-surface sources the incident wave illuminates a large area of the basement (the 'Fresnel area'), and furthermore, arrivals over a range of incident angles have sufficiently similar travel times to contribute to the crustal shear waves seen on marine profiles; if the phase angle of the converted shear wave varied rapidly with angle of incidence we might expect destructive interference between arrivals with similar travel times, but since the phase angle varies so little with angle of incidence the phase of the converted shear waves will be stable even over normal oceanic crust where the basement velocity is likely to be laterally variable.

3.2 BASEMENT WITH VARIABLE S -WAVE VELOCITY

The top of the volcanic basement is typically broken up by numerous faults and cracks, frequently contains many void spaces created by pillow lavas and breccias and often has suffered weathering from prolonged interaction with sea-water. These factors all serve to change the mean Poisson's ratio of the basement from that of the fresh matrix rock.

Fig. 3 shows curves of the two-way energy transmission coefficient for a range of S -wave velocities in the basement with a constant basement P -wave velocity of 4.5 km s^{-1} . The major effect of reducing the basement shear velocity is to broaden the minimum in conversion efficiency at incident phase velocities around α_2 .

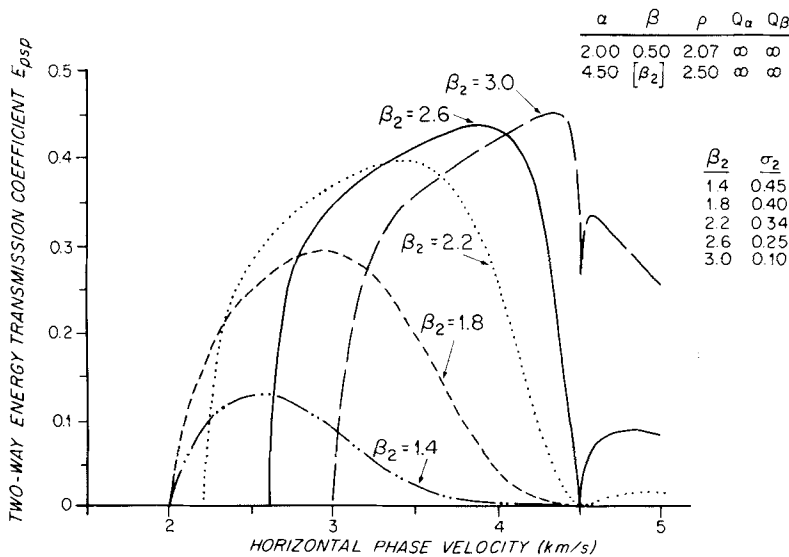


Figure 3. Basement with variable S -wave and constant P -wave velocities beneath unconsolidated sediment. Two-way energy transmission coefficient is shown for an interface between two half-spaces. Note that as the basement S -wave velocity decreases (increasing Poisson's ratio), the efficiency of conversion decreases markedly at phase velocities typical of lower crustal shear waves. The effect of both cracking or fracturing and of weathering on the volcanic basement is to lower the S -wave velocity, and thus reduce the energy in lower crustal shear phases.

At the top of the basement the P -wave velocity typically lies between 3 and 5 km s⁻¹, corresponding closely to the range of S -wave velocities in the crust. This means that the broad low in the efficiency of mode conversion centred on phase velocities around α_2 may prevent the occurrence of strong doubly converted crustal S -waves. Basement P -wave velocities increase with age over the first 20–40 Myr after formation at a spreading centre (Houtz & Ewing 1976), so we might expect to see some age dependence of converted shear energy from the lower crust.

Porosities as high as 40 per cent have been inferred for the upper part of the volcanic basement (Whitmarsh 1978; Kirkpatrick 1979), and it is likely that the velocity gradient observed in layer 2 is primarily caused by a downward decrease in crack density (Whitmarsh 1978; Spudich 1979; White & Matthews 1980; Stephen *et al.* 1980). A number of theoretical approaches are available to calculate the seismic velocities of a cracked solid (Anderson, Minister & Cole 1974), although the large number of variables such as the crack orientations and size distribution, their aspect ratios, the extent to which they interact, the properties and pressure conditions of the infilling media, the propagation azimuth and the seismic wave frequency render the theoretical results approximations, at best, to the real crust.

With reasonable assumptions about the likely distribution of void space O'Connell & Budiansky's (1974, 1977), interactive theory suggests that the Poisson's ratio of the volcanic basement will in general be increased (α/β is increased), by cracks. It is possible for the presence of cracks to cause a decrease in Poisson's ratio, but only if the cracks are dry or less than about two-thirds saturated with water, an unlikely occurrence in the top of the volcanic basement.

Seismic velocities measured in the laboratory on samples of basalt indicate that weathering of the crust as it becomes older causes the P -wave velocity to decrease and the Poisson's ratio to rise to as high as 0.37 (Christensen & Salisbury 1972; 1973).

Shear wave arrivals from layer 2 are rarely observed partly because lateral variations in the seismic velocity structure and topography may cause large amplitude variations and destroy their coherency as discussed in this paper and partly because, even where they are present, they are generally submerged in other returns on marine seismic profiles. However, the few velocities that have been reported support Poisson's ratios in layer 2 of approximately 0.27 to 0.30 (Helmberger & Morris 1970; Sutton, Maynard & Hussong 1971; Spudich *et al.* 1978, 1980).

An increase in the amount of fracturing or weathering of the basement not only causes the Poisson's ratio to increase, but also generally decreases the overall P -wave velocity and raises the absorptivity (O'Connell & Budiansky 1977). The first two effects both reduce the efficiency of conversion of lower crustal shear waves, whilst increased absorptivity further reduces the amplitude of shear waves propagating into the crust. Thus the degree of fracturing and weathering in the uppermost volcanic basement may be an important control on whether we observe doubly converted S -waves.

Fracturing and weathering may increase the Poisson's ratio in the basement to perhaps as high as 0.40, but even so there is still appreciable P – S conversion at some phase velocities (Fig. 3). The only way in which the apparent Poisson's ratio can be raised still higher, thus drastically reducing mode conversion, is if there is a thin transition zone at the top of the basement as discussed in Section 5. If the basement Poisson's ratio is 0.25 or only a little greater, the narrow minimum in conversion efficiency near α_2 will have little effect on the likelihood of observing converted shear waves on refraction profiles. This follows because, first, contributions to most crustal seismic returns, be they wide angle reflections or interference head waves, come from a range of phase velocities, and if the minimum in the transmission coefficient is narrow only a few of the contributory raypaths will be affected.

Secondly, in the real crust the basement velocity is likely to vary laterally, as is the dip of the basement (as the scale of angle of incidence on Fig. 2(a) shows, even small dips cause large changes in the horizontal phase velocity at which the transmission coefficient drops to zero); this means that no one phase velocity is consistently filtered out.

3.3 SEDIMENT WITH VARIABLE S-WAVE VELOCITY

We next consider the effect of varying just the sediment S -wave velocity β_1 while maintaining the P -wave velocity α_1 at 2.0 km s^{-1} . For any given constant basement properties the two-way energy transmission coefficient exhibits a simple progression from maximum conversion when β_1 is zero, decreasing to progressively smaller values as β_1 is increased (Fig. 4). The largest changes occur where β_1 is small; in the example shown in Fig. 4 over 80 per cent of the incident energy is doubly converted between phase velocities of $3\text{--}4 \text{ km s}^{-1}$ when β_1 is zero, but only about 40 per cent when β_1 is 0.5 km s^{-1} , thereafter decreasing less rapidly to around 25 per cent when β_1 is 1.15 km s^{-1} (i.e. when sediment Poisson's ratio = 0.25).

Shear wave velocities in unconsolidated sediment may not be zero, but they may well be very small; Hamilton (1976) suggests that shear velocities may be as low as 0.1 km s^{-1} at the seafloor, increasing to around 0.4 km s^{-1} at 150 m sub-bottom and only reaching 0.6 km s^{-1} at 500 m depth. Thus considerable P - S conversion may occur when the basement is overlain by poorly consolidated sediment.

3.4 SEDIMENT WITH VARIABLE P-WAVE VELOCITY

If we consider the hypothetical case where we hold the sediment shear wave velocity at zero, almost perfect mode conversion occurs for real phase velocities less than α_2 when the sediment P -wave velocity is the same as the basement S -wave velocity (Fig. 5). When the

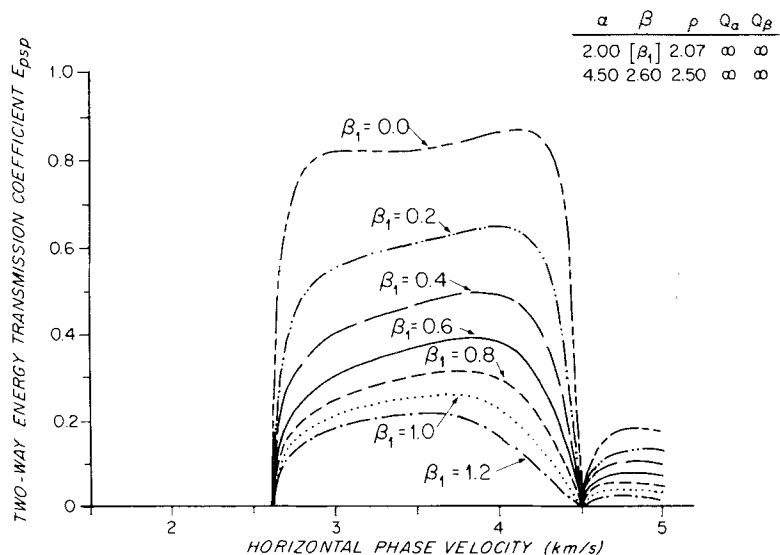


Figure 4. Sediment with variable S -wave and constant P -wave velocities. Two-way energy transmission coefficient is shown for an interface between two half-spaces. Note that the efficiency of conversion increases markedly as the sediment S -wave velocity decreases; thus more energy is doubly converted when the volcanic basement is overlain by unconsolidated sediment than when it is covered by consolidated sediment.

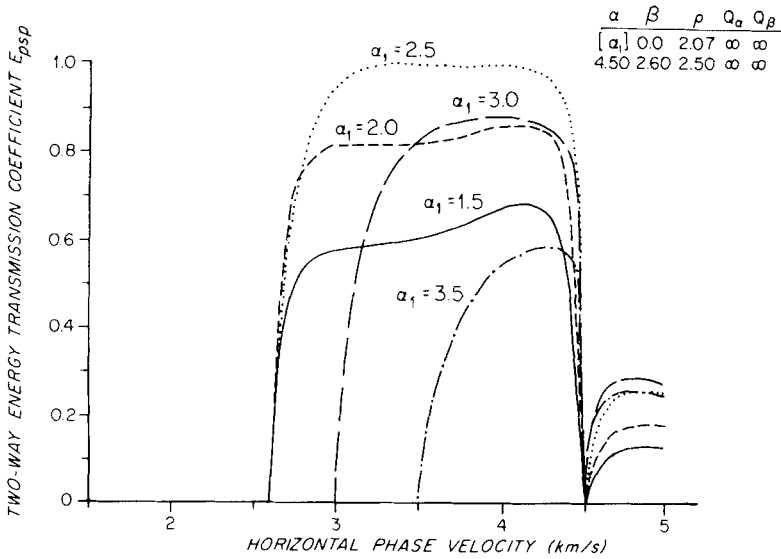


Figure 5. Sediment with variable *P*-wave and zero *S*-wave velocities. Two-way energy transmission coefficient is shown for an interface between two half-spaces. For this hypothetical case with zero sediment *S*-wave velocity, maximum conversion occurs when the sediment *P*-wave velocity equals the underlying basement *S*-wave velocity.

sediment *S*-wave velocity is not zero, but is nevertheless still small (as for unconsolidated sediments), maximum energy conversion still occurs when α_1 equals β_2 though as we demonstrated in Section 3.3 (Fig. 4), the maximum transmission coefficient reached is greatly reduced as β_1 increases from zero.

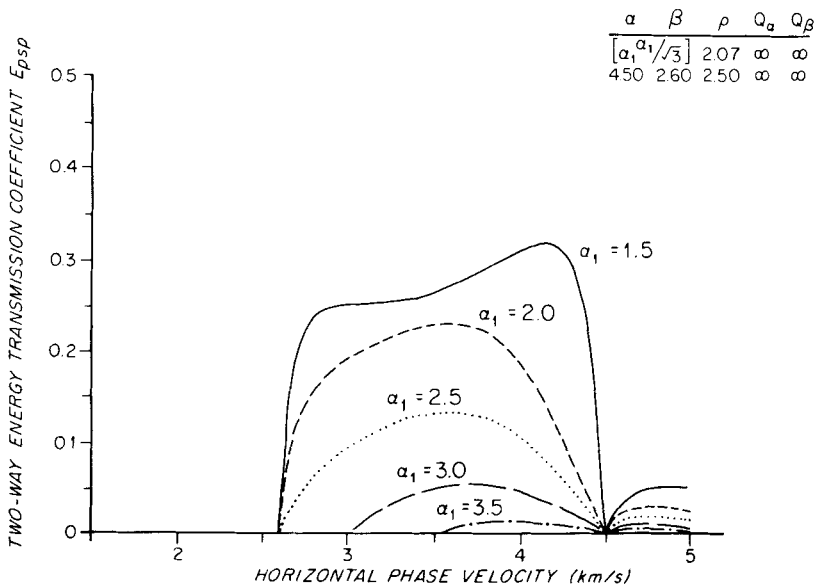


Figure 6. Sediment with variable velocities but constant Poisson's ratio of 0.25. Two-way energy transmission coefficient is shown for an interface between two half-spaces. Note that as the sediment velocities increase the efficiency of conversion decreases.

For well consolidated sediment, where we have assumed the Poisson's ratio to be 0.25, there is a simple progression of reducing efficiency of P - S conversion as the sediment velocities increase (Fig. 6).

3.5 EFFECT OF ABSORPTIVITY

The effect of absorption on the two-way conversion efficiency can be approximated by making the seismic velocities complex (Schwab & Knopoff 1972; Kennett 1975; Fryer 1978), provided the quality factor is independent of frequency and is large compared to unity. Adopting reasonable values of absorption in the sediments and upper crustal rocks (see, e.g. Hamilton 1972), causes little change in the energy conversion coefficients other than some smoothing of the sharp transitions near the P - and S -wave critical angles controlled mainly by the magnitude of the basement S -wave absorptivity.

4 Variable angle P -wave reflections from the basement with a transition zone at the top

The top of the volcanic basement is not always a first-order discontinuity at seismic wavelengths, as assumed in Section 3, but may be better represented by a transition zone over which the velocities vary with depth. We have assumed in our synthetic seismogram models that the seismic velocities in the transition zone increase with depth since this is a normal result of surface weathering and the reduction with depth of void space caused by pillow lavas, vesicles, breccias and fractures. There are certainly likely to be fine-scale velocity inversions and thin low or high velocity layers caused, for example, by interbedded sediments or basalt sills in the upper basement, but such layers are unlikely to be laterally continuous over distances comparable to the Fresnel area; their net effect is simply to change the mean seismic properties sensed by the incident wave.

We have modelled the response of a transition zone in the uppermost basement using the full wave reflectivity method (Fuchs & Muller 1971). This method calculates the complete response, including all multiple reflections and interconversions, of a stack of plane, homogeneous and isotropic layers within the reflectivity zone. Rays are traced through the overlying source and receiver zones with allowance for absorption, geometric spreading and transmission losses, but without considering any multiple paths or interconversions (Kennett 1976). We have placed the top of the reflectivity zone just beneath the water-sediment interface so that the complete seismic return from the basement is calculated, but for clarity the seafloor reflection is omitted from the synthetic seismograms. We also do not calculate surface waves, so the 'pseudo-Rayleigh wave' from the ocean bottom discussed by Spudich & Helmberger (1979) is absent from our seismograms. A near surface source and hydrophone receiver are assumed.

We have represented velocity gradients in our models by a staircase of thin layers; this is a good approximation provided all multiples are included (Burdick & Orcutt 1979), and provided the thickness of the layers is much less than the smallest seismic wavelength. The validity of using thin homogeneous layers to model a velocity gradient was confirmed by checking that the seismograms converged to the same waveforms when the number of layers in the transition zones was changed. One special case which is easily tested is that identical synthetic seismograms are produced by a first order discontinuity and by a very thin layered transition zone at the top of the basement.

The waveform used in all the examples is a simple analytic signal with a dominant frequency of 10 Hz. The phase window for the calculations is 1.9–150 km s⁻¹, the high upper limit ensuring that seismograms at short ranges are well modelled (Stephen 1977).

The variable angle reflection seismograms resulting from different transition zone thicknesses, Δh , can be characterized by three main classes, distinguished by the magnitude of Δh compared to the seismic compressional and shear wavelengths, λ_α and λ_β respectively. In all the synthetic seismogram models the transition zone is a uniform gradient from the sediment velocities above ($\alpha = 2.0, \beta = 0.5 \text{ km s}^{-1}$), to typical volcanic basement velocities beneath ($\alpha = 4.5, \beta = 2.6 \text{ km s}^{-1}$).

4.1 FIRST-ORDER INTERFACE, $\Delta h = 0$

At a first-order interface between sediment and volcanic basement the coupling from incident *P*-wave to transmitted *S*-wave is so good that little *P*-wave energy is reflected at angles of incidence between the *P*-wave critical angle θ_α and the *S*-wave critical angle, θ_β (see solid line in Fig. 7). The *P*-wave reflection coefficient exhibits a small spike near θ_α , but only increases to a value near unity for angles of incidence greater than θ_β . This behaviour is in marked contrast to the case where *S*-wave velocities are small when the reflection coefficient rises steeply to unity at the critical angle, and remains high for all supercritical angles (see dashed line in Fig. 7).

The synthetic seismogram for a hydrophone shows marked minima on the traces at 7 and 9 km range in the wide angle basement reflection between the *P*- and *S*-wave critical distances (Fig. 9a). Our model includes a velocity gradient of 1.0 s^{-1} within the basement (Fig. 8) which is typical of seismic layer 2 and which gives a strong interference head wave (*P* in Fig. 9). A high amplitude doubly converted shear wave from the basement is also

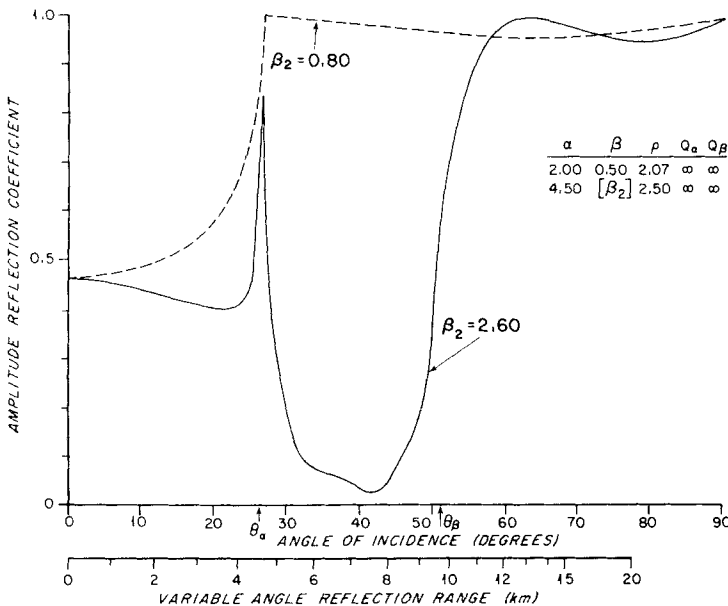


Figure 7. Compressional wave amplitude reflection coefficient versus angle of incidence for a *P*-wave incident on an interface between two half-spaces. The upper half-space has the properties of sediment and the lower half-space represents the volcanic basement. Solid line has $\beta_2 = 2.60 \text{ km s}^{-1}$ which is appropriate for the first-order discontinuity ($\Delta h = 0$, Fig. 9a); dashed line has $\beta_2 = 0.8 \text{ km s}^{-1}$ which is appropriate for the transition zone width greater than $\lambda_{\beta/2}$ ($\Delta h = 42 \text{ m}$, Fig. 9b). θ_α and θ_β are the *P*- and *S*-wave ray theoretical critical angles. Distance scale along the bottom is the variable angle reflection range in the models used to construct the synthetic seismograms in Fig. 9.

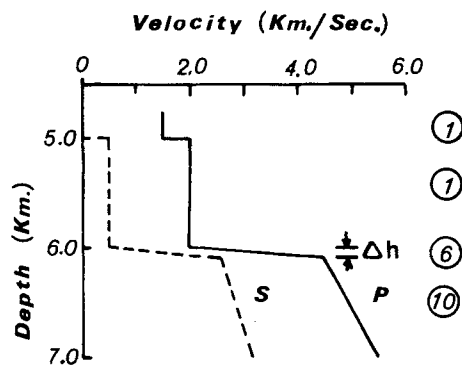


Figure 8. Velocity–depth diagram for P -wave reflections from basement. Δh is the thickness of the transition zone from sediment to basement velocities. The circled numbers to the right of the diagram are the number of layers used to approximate the gradients in the synthetic seismogram calculations. Solid line labelled 'P' is the P -wave velocity structure, dashed line labelled 'S' is the S -wave velocity structure.

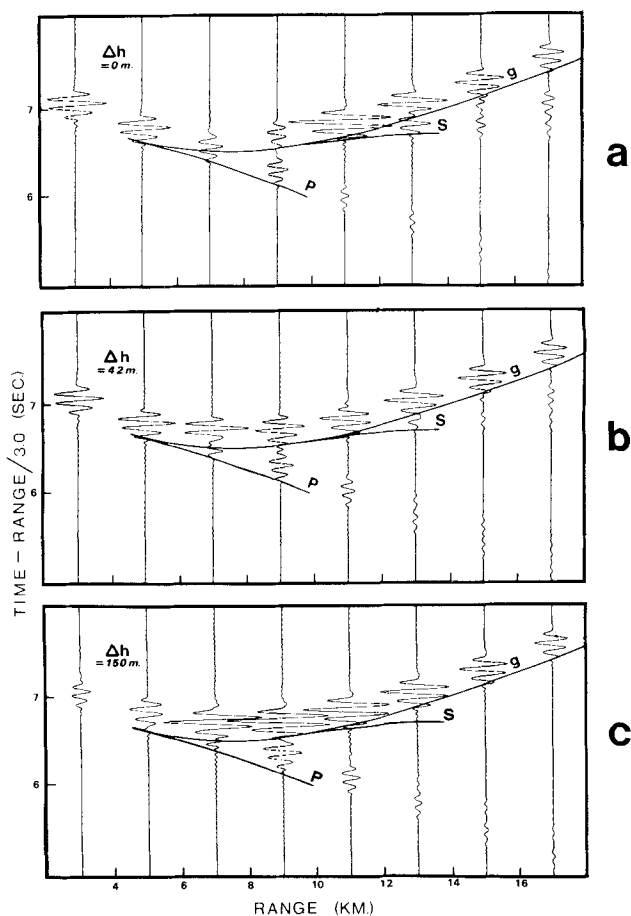


Figure 9. Synthetic seismograms for P -wave reflections from basement with different transition zone thicknesses (Δh). The velocity model is shown in Fig. 8. P -wave reflections from the top of basement are designated g and P - and S -wave arrivals from upper basement are designated P and S respectively. No scaling factors have been applied to the amplitudes.

produced (S in Fig. 9) as expected from the foregoing discussion of transmission coefficients (see solid line on Fig. 3). For this particular model and source signal the maximum reflection amplitude is offset about 2 km beyond the ray-theoretical S -wave critical distance; a lower frequency signal, a smaller velocity contrast or a shallower reflector would cause a larger offset (Červený 1967).

4.2 THIN TRANSITION ZONE, $\lambda_{\beta}/2 < \Delta h = 42 \text{ m} < \lambda_{\alpha}/2$

In Fig. 9(b) we have inserted a 42 m thick transition zone at the top of the basement, the effect of which is to markedly change the appearance of the seismogram by producing amplitude maxima in the wide angle reflections between 7 and 9 km, at just the ranges where the first-order interface caused amplitude minima. This can be explained by noting that the transition zone thickness ($\Delta h = 42 \text{ m}$) is greater than half the shear wavelength ($\lambda_{\alpha} = 230 \text{ m}$) in the top layer of the transition zone. Thus the basement appears sharp to P -waves but as a smooth gradient to S -waves, so it can be characterized as an interface with $\alpha_2 = 4.5 \text{ km s}^{-1}$ (the P -wave velocity in the bottom of the transition zone), but $\beta_2 = 0.8 \text{ km s}^{-1}$ (the S -wave velocity in the top layer) giving an unusually large apparent Poisson's ratio. The reflection coefficient versus angle of incidence curve for these values shown by the dashed line in Fig. 7 remains near unity for all angles greater than the P -wave critical angle θ_{α} . The amplitudes of doubly converted shear waves (S on Fig. 9) are greatly reduced compared to the first-order interface model, again as predicted by the transmission coefficient curves with large Poisson's ratio in the lower half space (e.g. Fig. 3).

The importance of this observation is that very fine velocity structure on the scale of only half the shear wavelength at the top of the basement may have an enormous effect on the variable angle P -wave reflection amplitudes even though we are considering seismograms produced solely by incident and reflected compressional waves. Although the incident and reflected wavelengths of the seismic signal are over 200 m, a change of only a few metres to a few tens of metres in the basement transition zone thickness can radically alter the seismogram. We have confirmed that the shear-wave velocity structure is solely responsible for the marked changes between Fig. 9(a) and (b) in the P -wave seismograms by producing the same synthetics as Fig. 9(b) with a model having a transition zone with a uniform basement P -wave velocity of 4.5 km s^{-1} but a gradient in the S -wave velocities. Thus even though we may only be interested in P -wave returns, we cannot model their amplitudes unless we also know the S -wave velocity structure in fine detail.

4.3 THICK TRANSITION ZONE, $\lambda_{\beta/2} \ll \lambda_{\alpha/2} < \Delta h = 150 \text{ m}$

When a step in velocity at the basement is replaced by a velocity gradient over more than half a wavelength, the pre-critical reflection amplitudes are greatly attenuated, but the supercritical wide angle reflections are little changed (Fuchs 1970; Braile & Smith 1975; White 1979). Such an effect can be seen in the seismogram in Fig. 9(c) produced by a 150 m thick transition zone. Other changes are that there are no discernible doubly converted shear waves and that the compressional basement head wave is slightly enhanced because the velocity gradient in the transition zone improves P -wave coupling into the basement (Spudich & Helmberger 1979).

5 Crustal shear waves doubly converted at the basement with a transition zone at the top

The general characteristics of shear wave conversion in a transition zone comprising a uniform gradient from the sediment to the upper basement velocities have already been

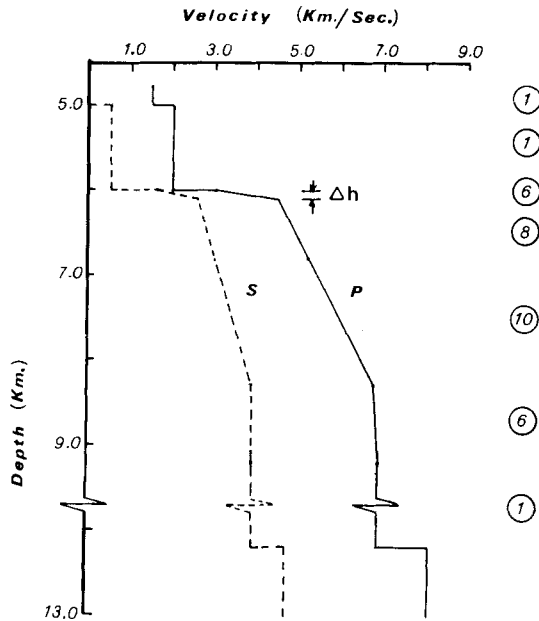


Figure 10. Velocity–depth diagram for P - to S -wave conversion at the top of basement. Δh is the thickness of the transition zone from low to high basement velocities. The circled numbers are the number of layers used to approximate the gradients in the synthetic seismogram calculations. Solid line labelled ‘ P ’ is the P -wave velocity structure, dashed line labelled ‘ S ’ is the S -wave velocity structure.

described in Section 4, so we have used a perhaps more realistic model to further describe the effects on shear wave production of fine-scale velocity structure in the uppermost basement. Our model (Fig. 10) consists of a combination of a first-order step in seismic properties at the sediment–basement interface (from the sediment with $\alpha = 2.0 \text{ km s}^{-1}$, $\beta = 0.5 \text{ km s}^{-1}$, $\rho = 2.07 \text{ g m}^{-3}$ to basement with $\alpha = 3.0 \text{ km s}^{-1}$, $\beta = 1.6 \text{ km s}^{-1}$, $\rho = 2.50 \text{ g cm}^{-3}$), combined with an underlying transition zone of thickness Δh in which the velocities increase smoothly to the same basement velocities as we assumed in Section 4 ($\alpha = 4.5 \text{ km s}^{-1}$, $\beta = 2.6 \text{ km s}^{-1}$). The remaining velocity structure represents a normal oceanic crustal section, with a uniform velocity gradient of 1.0 s^{-1} in layer 2 underlain by a much lower gradient in layer 3, and a step in velocity to a uniform upper mantle with $\alpha = 8.1 \text{ km s}^{-1}$, $\beta = 4.5 \text{ km s}^{-1}$. The travel times of doubly converted shear waves returned from these crustal layers are superimposed on the seismograms in Fig. 11.

5.1 FIRST-ORDER INTERFACE, $\Delta h = 0$

As we noted in Section 4.1, strong converted shear waves (S) are produced at a first-order discontinuity (Fig. 11a). High amplitude intracrustal multiples (SS) result from reflection of the upward travelling shear wave at the sharp basement interface. The amplitudes of shear wave refractions are largely governed by the same factors as control compressional wave refractions; for example, velocity gradients enhance the amplitudes by generating interference head waves. There are, however, major differences between P - and S -wave energy returned by the lower crust as wide angle reflections. The efficiency of mode conversion at the basement interface is strongly dependent on the horizontal phase velocity of the wave, as demonstrated in Section 3. The doubly converted shear wave reflection will be selectively

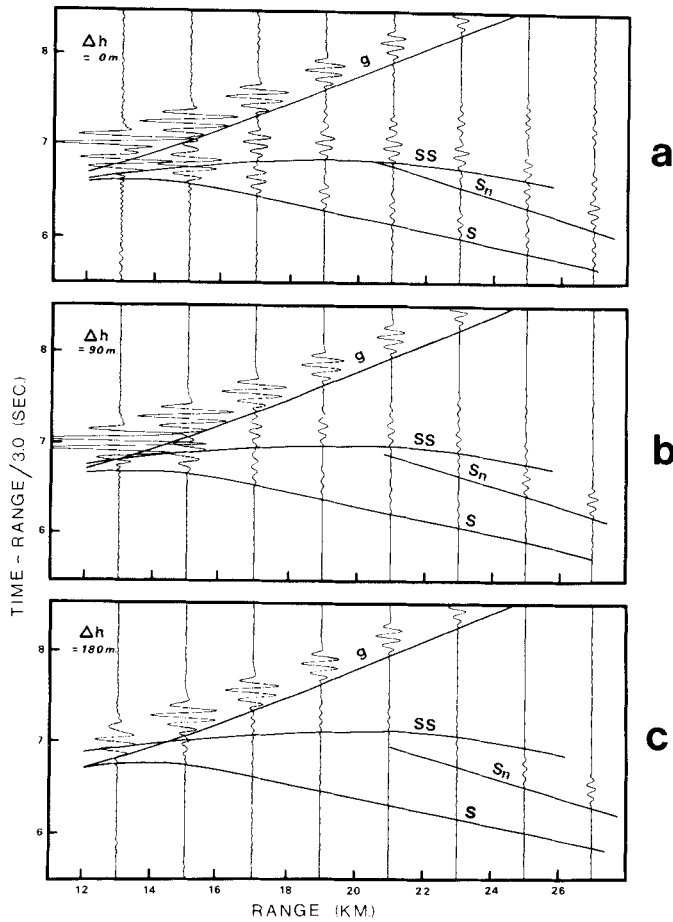


Figure 11. Synthetic seismograms for P - and S -wave conversion at the top of basement for different transition zone thicknesses (Δh). The velocity model is shown in Fig. 10. P -wave reflections from the top of basement are designated g and S -wave arrivals from the crust and from the Moho are designated S and S_n . SS is a crustal multiple reflected from below the basement–sediment interface. No scaling factors have been applied to the amplitudes.

absent over those portions of the hyperbolic wide angle reflection curve where the horizontal phase velocity is such that conversion efficiency is low. In general, conversion is poorest at high horizontal phase velocities (small angles of incidence), decreasing to zero at normal incidence, so shear reflections usually disappear as the range decreases. Wide angle reflected energy is generally a significant part of the energy returned from the lower crust, so the variations in conversion efficiency have a strong control on the distribution of converted shear wave energy. In Fig. 11(a), the wide angle Moho reflection S_n rapidly decreases in amplitude as it is traced to decreasing range, disappearing altogether at sub-critical ranges (phase velocities above 4.5 km s^{-1}).

5.2 THIN TRANSITION ZONE, $\lambda_{\beta/2} < \Delta h = 90 \text{ m} < \lambda_{\alpha/2}$

As the transition zone thickness, Δh is increased from zero there is no major change in the transmitted shear wave seismogram until Δh reaches about 90 m. This confirms our earlier comment based on the variable angle reflection amplitudes that a transition zone appears to

be like a first-order discontinuity when its thickness is less than half both the P - and S -wavelengths at the top of the transition zone, even though we are only considering incident P -waves. The S -wave velocity at the top of the basement is 1.6 km s^{-1} (Fig. 10), corresponding to a wavelength of 160 m with the 10 Hz signal. When Δh is 90 m the transition zone appears as a first-order interface at P -wavelengths but as a gradient at S -wavelengths, so we can consider the transition zone as responding to incident P -waves in a manner similar to a first-order interface with $\alpha = 4.5 \text{ km s}^{-1}$, $\beta = 1.6 \text{ km s}^{-1}$. As demonstrated by Fig. 3, shear wave conversion at an interface beneath which there is such a high apparent Poisson's ratio is still good at low horizontal phase velocities, but decreases as the phase velocity increases. The resultant seismogram (Fig. 11b) exhibits attenuated layer 3 returns (S) compared to those produced by a first-order interface (Fig. 11a). Conversion at phase velocities appropriate for the mantle S -wave reflection (S_n) occurs primarily at the step in properties at the base of the sediments rather than in the upper basement transition zone, and consequently changes in the transition zone thickness have little effect on the mantle reflection amplitudes.

An interesting corollary of the marked decrease in the amplitude of the layer 3 converted S -wave return which occurs when the transition zone thickness is greater than half a shear wavelength is that a basement transition zone may act as a low-pass frequency filter. A transition zone over a fixed thickness will appear as a gradient to high frequency incident waves, giving poor conversion, but will appear sharp to sufficiently low frequency waves, thereby generating large converted S -waves.

5.3 THICK TRANSITION ZONE, $\lambda_{\beta/2} < \lambda_{\alpha/2} < \Delta h = 180 \text{ m}$

When the transition zone thickness is greater than both the P - and the S -wavelengths, no mode conversion occurs in the gradient. In our model (Fig. 10) the P - S conversion will occur only at the step in velocities at the base of the sediments; the two-way energy transmission coefficient as a function of horizontal phase velocity for this particular case is illustrated by the dash-dot-dash line in Fig. 2. Shear waves at low phase velocities typical of layer 2 have the highest conversion efficiency and layer 2 returns are still clear on Fig. 12(a). Conversion efficiency is decreased at greater phase velocities typical of lower crustal returns, resulting in a barely discernible layer 3 head wave (S on Fig. 11a). The mantle reflection, S_n , is relatively stronger than the layer 3 return because, as is normal, the supercritical reflection off the sharp Moho discontinuity has a higher amplitude than the interference head wave from the small velocity gradient in layer 3; the conversion efficiency for the two arrivals is approximately the same (Fig. 2a).

6 Conclusions

The fine-scale shear wave velocity structure at the top of the oceanic volcanic layer may exert considerable control on the character of the seismograms; this is true even if we only consider compressional wave energy incident on and returned from the crust. Our main conclusions are:

(a) The efficiency of mode conversion at a sharp interface varies with the horizontal phase velocity, decreasing to zero at a phase velocity equal to the basement P -wave velocity and generally remaining low at phase velocities higher than the basement P -wave velocity. Most efficient conversion usually occurs at phase velocities lower than the basement P -wave velocity, or to express it in terms of angle of incidence, between the basement P - and S -wave critical angles.

(b) At a first-order interface between sediment and basement, the efficiency of mode conversion decreases as the sediment velocities are raised if we assume a constant Poisson's ratio of 0.25 in the sediment (which is appropriate for consolidated sediment). Considerably better conversion occurs if the sediment *S*-wave velocity is very low (i.e. high Poisson's ratio) as is frequently the case in unconsolidated sediment. Changes in the sediment type overlying basement are likely to be regionally controlled, so consequently they may exert a regional influence on the presence or absence of converted shear waves.

(c) Conversion efficiency is reduced, particularly at horizontal phase velocities around the basement *P*-wave velocity, by raising the Poisson's ratio in the basement. Effects at the top of the basement such as weathering or the presence of void space in pillow lavas, rubble, cracks and fractures all tend to increase Poisson's ratio and therefore to decrease mode conversion. Lateral changes in the basement velocity and in the local dip of the sediment–basement interface are likely to be much more localized than variations in the overlying sediment and may cause considerable variation in doubly converted *S*-wave amplitudes along a single seismic profile.

(d) If the sharp interface at the top of the basement is replaced by a thin transition zone over which the velocities increase with depth, it is found that the transition gradient appears as a first-order interface to incident waves if its thickness is less than half a wavelength. Furthermore the relevant *P*-wave velocity structure is that obtained by dividing the *P*-wave velocity in the top layer of the transition zone by the source frequency. Similarly, the relevant wavelength for the *S*-wave velocity structure depends on the wavelength of *S*-waves in the top layer of the transition zone. Even though we are only considering the seismogram produced by *P*-waves incident on and returned from the crust, the *S*-wave velocity structure strongly effects the amplitudes of both reflections and refractions. As we have documented in this paper, changes of only a few metres to a few tens of metres in the *S*-wave transition zone thickness may cause major differences in the *P*-wave amplitudes even though the thickness changes are on a scale much smaller than the wavelength of the incident and returned *P*-waves.

Acknowledgments

We are grateful to Paul Spudich for sending us a copy of his PhD thesis, and acknowledge his insight in first showing that the relationship between the efficiency of shear wave conversion and the seismic velocities at an interface is most clearly demonstrated by plotting the transmission coefficient as a function of the horizontal phase velocity. G. M. Purdy and two anonymous referees provided helpful criticism.

This work was supported by the Ocean Science and Technology Division of the Office of Naval Research through contract N00014-74-C0262 NR-083-004. RSW acknowledges support from a Woods Hole Oceanographic Institution postdoctoral scholarship. Woods Hole Oceanographic Institution Contribution Number: 4470.

References

- Anderson, D. L., Minister, B. & Cole, D., 1974. The effect of oriented cracks on seismic velocities, *J. geophys. Res.*, **79**, 4011–4015.
- Braile, L. W. & Smith, R. B., 1975. Guide to the interpretation of crustal refraction profiles, *Geophys. J. R. astr. Soc.*, **40**, 145–176.
- Burdick, L. J. & Orcutt, J. A., 1979. A comparison of the generalized ray and reflectivity methods of waveform synthesis, *Geophys. J. R. astr. Soc.*, **58**, 261–278.
- Červený, V., 1967. The amplitude–distance curves for waves reflected at a plane interface for different frequency ranges, *Geophys. J. R. astr. Soc.*, **13**, 187–196.

- Červený, V. & Ravindra, R., 1971. *Theory of Seismic Head Waves*, University of Toronto Press, Toronto, Canada.
- Christensen, N. I. & Salisbury, M. H., 1972. Seafloor spreading, progressive alteration of layer 2 basalts, and associated changes in seismic velocities, *Earth planet. Sci. Lett.*, **15**, 367–375.
- Christensen, N. I. & Salisbury, M. H., 1973. Velocities, elastic moduli and weathering – age relations for Pacific layer 2 basalts, *Earth planet. Sci. Lett.*, **19**, 461–470.
- Christensen, N. I. & Salisbury, M. H., 1975. Structure and composition of the lower oceanic crust, *Rev. Geophys. Space Phys.*, **13**, 57–86.
- Cook, K. L., Algermissen, S. T. & Costain, J. K., 1962. The status of *PS* converted waves in crustal studies, *J. geophys. Res.*, **67**, 4769–4778.
- Davies, E. E., Lister, C. R. B. & Lewis, B. T. R., 1976. Seismic structure of the Juan de Fuca Ridge: Ocean bottom seismometer results from the median valley, *J. geophys. Res.*, **81**, 3541–3555.
- Ewing, M., Sutton, G. H. & Officer, Jr, C. B., 1954. Seismic refraction measurements in the Atlantic Ocean, part IV, *Bull. seism. Soc. Am.*, **44**, 21–38.
- Ewing, J. I. & Ewing, M., 1959. Seismic refraction measurements in the Atlantic Ocean basins, Mediterranean Sea, Mid-Atlantic Ridge and Norwegian Sea, *Bull. geol. Soc. Am.*, **70**, 291–318.
- Fowler, C. M. R., 1976. Crustal structure of the Mid-Atlantic ridge crest at 37° N, *Geophys. J. R. astr. Soc.*, **47**, 459–492.
- Francis, T. J. & Shor, G. G., 1966. Seismic refraction measurements in the NW Indian Ocean, *J. geophys. Res.*, **71**, 427–449.
- Fryer, G. J., 1978. Reflectivity of the ocean bottom at low frequency, *J. acoust. Soc.*, **67**, 35–42.
- Fuchs, K., 1970. On the determination of velocity–depth distribution of elastic waves from the dynamic characteristics of the reflected wave field, *Z. geophys.*, **36**, 531–568.
- Fuchs, K. & Muller, G., 1971. Computation of synthetic seismograms with the reflectivity method and comparison with observations, *Geophys. J. R. astr. Soc.*, **23**, 417–433.
- Hamilton, E. L., 1972. Compressional wave attenuation in marine sediments, *Geophysics*, **37**, 620–646.
- Hamilton, E. L., 1976. Shear-wave velocity versus depth in marine sediments: a review, *Geophysics*, **41**, 985–996.
- Helmberger, D. V. & Morris, G. B., 1970. A travel time and amplitude interpretation of a marine refraction profile: transformed shear waves, *Bull. seism. Soc. Am.*, **60**, 593–600.
- Houtz, R. E. & Ewing, J. I., 1976. Upper crustal structure as a function of plate age, *J. geophys. Res.*, **81**, 2490–2498.
- Katz, S. & Ewing, M., 1956. Seismic refraction velocities in the Atlantic Ocean, part VII, *Bull. geol. Soc. Am.*, **67**, 475–510.
- Kennett, B. L. N., 1975. The effects of attenuation on seismograms, *Bull. seism. Soc. Am.*, **65**, 1643–1651.
- Kennett, B. L. N., 1976. Theoretical seismogram calculation for laterally varying crustal structures, *Geophys. J. R. astr. Soc.*, **42**, 579–589.
- Kirkpatrick, R. J., 1979. The physical state of the oceanic crust: results of downhole geophysical logging in the Mid-Atlantic Ridge at 23° N, *J. geophys. Res.*, **84**, 178–188.
- Lewis, B. T. R. & McClain, J., 1977. Converted shear waves as seen by ocean bottom seismometers and surface buoys, *Bull. seism. Soc. Am.*, **67**, 1291–1302.
- Ludwig, W. J., Den, N. & Murauchi, S., 1973. Seismic reflection measurements of southwest Japan margin, *J. geophys. Res.*, **78**, 2508–2516.
- Murauchi, S., Den, N., Asano, S., Hotta, H., Yoshii, T., Asanuma, T., Hagiwara, K., Ichikawa, K., Sato, T., Ludwig, W. J., Ewing, J. I., Edgar, N. J. & Houtz, R. E., 1968. Crustal structure of the Philippine Sea, *J. geophys. Res.*, **73**, 3143–3171.
- O'Connell, R. J. & Budiansky, B., 1974. Seismic velocities in dry and saturated cracked solids, *J. geophys. Res.*, **79**, 5412–5425.
- O'Connell, R. J. & Budiansky, B., 1977. Viscoelastic properties of fluid-saturated cracked solids, *J. Geophys. Res.*, **82**, 5719–5735.
- Officer, C. B., Ewing, M. & Wuenschel, P. C., 1952. Seismic refraction measurements in the Atlantic Ocean, part IV, Bermuda, Bermuda Rise and Nares Basin, *Bull. geol. Soc. Am.*, **63**, 777–808.
- Purdy, G. M. & Detrick, R. S., 1978. A seismic refraction experiment in the central Banda Sea, *J. geophys. Res.*, **83**, 2247–2258.
- Schwab, F. A. & Knopoff, L., 1972. Fast surface wave and free mode computations, *Meth. comput. Phys.*, ed. Bolt, B. A., **11**, 87–180.
- Spudich, P. A., 1979. Oceanic crustal studies using waveform analysis and shear waves, *PhD dissertation*, University of California at San Diego.

- Spudich, P. K. P., Salisbury, M. H. & Orcutt, J. A., 1978. Ophiolites found in oceanic crust? *Geophys. Res. Lett.*, **5**, 341–344.
- Spudich, P. K. P. & Helmberger, D. V., 1979. Synthetic seismograms from model ocean bottoms, *J. geophys. Res.*, **84**, 189–204.
- Stephen, R. A., 1977. Synthetic seismograms for the case of the receiver within the medium, *Geophys. J. R. astr. Soc.*, **51**, 169–181.
- Stephen, R. A., Louden, K. E. & Matthews, D. H., 1980. The oblique seismic experiment on DSDP Leg 52, *Geophys. J. R. astr. Soc.*, **60**, 289–300.
- Sutton, G. H., Maynard, G. L. & Hussong, D. M., 1971. Widespread occurrence of a high velocity basal layer in the Pacific crust found with repetitive sources and sonobuoys, in The structure and physical properties of the Earth's crust, *Geophys. Monogr. Ser.*, **14**, 193–209, ed. Heacock, J. G., A.G.U., Washington, D.C.
- White, R. S., 1979. Oceanic upper crustal structure from variable angle seismic reflection–refraction profiles, *Geophys. J. R. astr. Soc.*, **57**, 683–726.
- White, R. S. & Matthews, D. H., 1980. Variations in oceanic upper crustal structure in a small area of the north-eastern Atlantic, *Geophys. J. R. astr. Soc.*, **61**, 401–435.
- Whitmarsh, R. B., 1978. Seismic refraction studies of the upper igneous crust in the North Atlantic and porosity estimates for Layer 2, *Earth planet. Sci., Lett.*, **37**, 451–464.